Clr4^{SUV39H1} ubiquitination and non-coding RNA mediate transcriptional silencing via heterochromatic phase transitions

Authors

Hyun-Soo Kim[1,4], Benjamin Roche[1,2], Sonali Bhattacharjee[1], Leila Todeschini[3], An-Yun Chang[1], Christopher Hammell[1], André Verdel[3], Robert A. Martienssen[1,4]*

Affiliations

[1] Cold Spring Harbor Laboratory, Cold Spring Harbor, New York 11724, USA.

[2] present address: University of North Dakota, School of Medicine & Health Sciences, 1301 N Columbia Rd. Stop 9037, Grand Forks, North Dakota 58202

[3] Institute for Advanced Biosciences, UMR InsermU1209/CNRS5309/UGA, University of Grenoble Alpes, Grenoble, France.

[4] Howard Hughes Medical Institute, Cold Spring Harbor Laboratory, Cold Spring Harbor, NY 11724, USA

*Corresponding author. Email: martiens@cshl.edu

Abstract

Transcriptional silencing by RNAi paradoxically relies on transcription, but how the transition from transcription to silencing is achieved has remained unclear. The Cryptic Loci Regulator complex (CLRC) in *Schizosaccharomyces pombe* is a cullin-ring E3 ligase required for silencing that is recruited by RNAi. We found that the E2 ubiquitin conjugating enzyme Ubc4 interacts with CLRC and mono-ubiquitinates the histone H3K9 methyltransferase Clr4^{SUV39H1}, promoting the transition from co-transcriptional gene silencing (H3K9me2) to transcriptional gene silencing (H3K9me3). Ubiquitination of Clr4 occurs in an intrinsically disordered region (IDR), which undergoes robust liquid-liquid phase separation (LLPS), along with Swi6^{HP1} the effector of transcriptional gene silencing. Phase separation of Clr4 and Swi6 is exquisitely sensitive to non-coding RNA (ncRNA), which promotes dimerization, chromatin association, and di-, but not tri-methylation instead. Ubc4-CLRC also targets the transcriptional co-activator Bdf2^{BRD4}, down-regulating centromeric transcription and small RNA production. The deubiquitinase Ubp3 counteracts both activities.

Main text

Heterochromatin has crucial roles in genome stability by silencing repetitive DNA and by suppressing recombination[1-7]. In the fission yeast *Schizosaccharomyces pombe*, the H3K9 methyltransferase Clr4, the homolog of mammalian SUV39H1 and SUVH39H2, methylates histone H3 lysine 9 (H3K9) to maintain centromeric heterochromatin during the cell cycle[8-10]. Centromeric non-coding RNA (ncRNA) is transcribed by RNA Pol II

during S phase, and is processed to make centromeric sRNA by the concerted action of the RNAi transcriptional silencing complex (RITS), the RNA-directed RNA Polymerase Complex (RDRC) and Dicer (Dcr1)[7,11-16]. Di-methylation of H3K9 by Clr4, guided in part by sRNA, mediates co-transcriptional gene silencing (CTGS) of heterochromatin, which remains permissive to transcription during S phase. The subsequent tri-methylation of H3K9 by Clr4 and strong binding of Heterochromatin Protein 1 (HP1) homologs Swi6 and Chp2, suppresses RNA Pol II-dependent ncRNA transcription via transcriptional gene silencing (TGS), which is essential for the epigenetic inheritance of heterochromatin[1,17-19]. However, the mechanism that promotes the transition from RNAi-dependent CTGS to TGS is unclear.

Ubiquitination can regulate enzyme activity by adding a single ubiquitin to its substrate (mono-ubiquitination), or target protein degradation via the 26S proteasome by the addition of a ubiquitin chain (poly-ubiquitination). Ubiquitination requires ubiquitin, an E1 ubiquitin activating enzyme, an E2 ubiquitin conjugating enzyme and an E3 ubiquitin ligase[20-23]. E2 enzymes interact with E1 and E3 enzymes and have essential roles in determination of ubiquitin linkage specificity and ubiquitin chain length[24]. The ubiquitination complex Cul4-Rik1^{Raf1Raf2} (CLRC) of *S. pombe* is composed of cullin Cul4, the RING-box protein Rbx1, the DNA damage binding protein 1 (DDB1) homolog Recombination in K 1 (Rik1) and two substrate receptors, Raf1 and Raf2, as well as the eponymous Clr4, which is only weakly associated *in vitro*[25-30]. Cul4 is a highly conserved E3 ligase and interacts with Rik1/Raf1/Raf2 for substrate recognition. All subunits of CLRC are essential for heterochromatin formation but its E2 enzyme and

ubiquitination targets are not well characterized[25-28].

We previously showed that a specific mutation in the E2 ubiquitin conjugating enzyme Ubc4 (*ubc4-G48D*) reduces heterochromatic silencing at centromeres, at the mating-type locus and at telomeres[31]. Overexpression of Ubc4 also causes chromosome mis-segregation[32]. We found that the *ubc4-G48D* (*ubc4-1*) mutation results in Ubc4 protein instability leading to an overall lower Ubc4 protein level (Extended Data Fig. 1a,c). Replacing *ubc4* with its mouse homolog *UBE2D2* fully complemented *ubc4-1*, while *mUBE2D2-G48D* (*mUBE2D2-1*) had similar silencing defects to *ubc4-1*, showing that the function of Ubc4 is likely conserved throughout evolution (Extended Data Fig. 1a,b). We also isolated a spontaneous second-site suppressor S137T, which re-stabilizes Ubc4-1 protein levels, thus restoring silencing (Extended Data Fig. 1d-f). The E3 ubiquitin ligase Cul4 is an essential subunit of the CLRC, and *cul4-GFP* (*cul4-1*) is a hypomorphic mutant with reduced heterochromatic silencing[27]. *ubc4-1* and the *cul4-1* mutants have very similar phenotypes, including loss of silencing of *ade6*$^+$ and *ura4*$^+$ reporter genes in centromeric heterochromatin, as well as increased binding of Rpb1, the main subunit of RNA polymerase II, to heterochromatin (Fig. 1a and Extended Data Fig. 1b) and increased production of siRNA (Fig. 1f). Interestingly, while H3K9me3 was lost from both *ubc4-1* and *cul4-1* mutants at all heterochromatic loci tested, H3K9me2 was increased at the centromeric *dg* and *dh* repeats (Fig. 1a and Extended Data Figs. 1g and 2a-c). Increased H3K9me2 was also observed at the centromeric *ade6*$^+$ reporter gene, which accumulates small RNA, but not at the *ura4*$^+$ gene, which does not (Extended Data Figs. 2a and 7a). The

Swi6^{HP1} protein, which coats and maintains heterochromatin, displayed intermediate binding levels at centromeres in *ubc4-1* and *cul4-1* mutants presumably because it recognizes both H3K9me2 and H3K9me3 (Extended Data Fig. 2d)[18,33]. In contrast, H3K9me2/3 and Swi6 were completely lost from both *ubc4-1* and *cul4-1* mutants at telomeres or mating-type loci where RNAi-dependent sRNA production is limited (Extended Data Fig. 2b-d).

To determine whether RNAi is important for maintaining H3K9me2 in *ubc4-1* mutant cells, we introduced the *ubc4-1* mutation in *dcr1Δ* mutant cells and found that the *dcr1Δ ubc4-1* double-mutant lost both H3K9me2 and H3K9me3 and was hyper-sensitive to the microtubule destabilizing agent thiabendazole (TBZ), showing that centromeric heterochromatin was completely disrupted similarly to the *clr4* deletion mutant (Fig. 1a and Extended Data Figs. 1b and 2e). The more severe alleles *ubc4-3xHA* and *cul4Δ* abolished H3K9me2 and H3K9me3 altogether indicating that *ubc4-1* and *cul4-1* are hypomorphic and they might have other targets important for heterochromatin silencing (Extended Data Fig. 2f,g). In addition to their similar phenotypes, we found that Ubc4 and Cul4 physically interact and form a stable complex by co-immunoprecipitation (Co-IP) (Extended Data Fig. 2h). Ubc4 also forms a complex with Raf1 and Raf2, two substrate receptors of CLRC (Extended Data Fig. 2i) that mediate recruitment by siRNA-to-chromatin 1 (Stc1) and the RNA-induced transcriptional gene silencing (RITS) complex. These results indicate that Ubc4 and Cul4 form the E2/E3 complex by which CLRC targets substrates important for H3K9 methylation, in a RNAi-dependent manner.

105 Next, we set out to identify the substrates of this novel E2/E3 complex, Ubc4-CLRC, for the regulation of H3K9 methylation. Interestingly, Clr4 co-purifies with the CLRC *in vivo*, but does not behave like a structural component of CLRC *in vitro*[25-28]. This led us to hypothesize that Clr4 is itself a target of the Ubc4-CLRC. Indeed, another Clr4 human homolog, SETDB1, is mono-ubiquitinated at its SET-Insertion domain and
110 this modification is important for its H3K9 methyltransferase activity[34,35]. To test whether Clr4 is a substrate of Ubc4-CLRC, we purified 3xFlag-Clr4 protein from *S. pombe* cells and detected a single higher molecular weight form that reacted with ubiquitin antibodies in a Ubc4-dependent fashion (Fig. 1b and Extended Data Fig. 3a,b). A pulldown of ubiquitinated proteins using Ubiquitination Affinity Beads (UBA) revealed a
115 similar higher molecular weight Clr4 which is also dependent on Ubc4 (Extended Data Fig. 3c). In addition to Ubc4, the presence of this higher molecular weight Clr4 depends on Cul4, Rik1, Raf1 and Raf2, the other components of CLRC, but not on the proteasome inhibitor MG-132 (Extended Data Fig. 3d,e). These results strongly suggest that Ubc4, together with CLRC, mono-ubiquitinates Clr4 *in vivo*.

120 We were unable to recover sufficient peptides *in vivo* for the identification of Clr4 ubiquitination sites by Mass Spectrometry because of the very low abundance of Clr4 in *S. pombe* cells[36], so instead we ubiquitinated 6xHis-Clr4 recombinant protein *in vitro*. Clr4 was mono-ubiquitinated efficiently by UBE2D3, the human homolog of Ubc4, independently of an E3 ligase complex (Fig. 2d and Extended Data Fig. 1a), similarly to
125 SETDB1[35,37]. This approach uncovered 9 possible ubiquitination sites, which mostly reside in the intrinsically disordered region (IDR) between the chromodomain (CD) and

the PreSET domain (Fig. 1c and Extended Data Fig. 4a-d) which is involved in nucleosome binding[38].

To identify which of these represent functional sites *in vivo*, we partitioned the 36 lysines of Clr4 into 6 subgroups, which we then systematically mutated into arginines (R). We also included a mutant of all 36 lysines (*AllKtoR*). The all-lysine mutant (*AllKtoR*) and the second block mutant (*2-8KtoR*), corresponding to the middle of the IDR, completely abolished Clr4 ubiquitination *in vivo* (Fig. 1c,d and Extended Data Fig. 4d,e), consistent with the results of *in vitro* ubiquitination and Mass Spectrometry. By this means, we could narrow down the possible sites to 4 lysines (*clr4-2-4KtoR*; K109, K110, K113, and K114) (Fig. 1c,d and Extended Data Fig. 4f-i). These lysines are organized in tandem and are therefore very likely to compensate for each other. Using ChIP-seq, we found that *clr4-AllKtoR* lost both H3K9me2 and H3K9me3, presumably by reduced enzymatic activity[39], while *clr4-2-8KtoR* and *clr4-2-4KtoR* mutants had the same increase of H3K9me2 and decrease of H3K9me3 seen in *ubc4-1* and *cul4-1* hypomorphic mutants (Fig. 1e and Extended Data Fig. 4j). In *ubc4-1* and *cul4-1* mutants, we observed more than 2-fold increase of centromeric sRNA, as previously observed for *cul4-1*, but *clr4-2-8KtoR* and *clr4-2-4KtoR* mutants did not change centromeric sRNA production (Fig. 1f)[40]. These results indicate that Clr4 mono-ubiquitination by Ubc4-CLRC complex mediates the transition from H3K9me2 to H3K9me3 (Fig. 1g).

Remarkably, the lysines in Clr4-2-8 co-incided precisely with two adjacent patches in the IDR that were previously shown to bind to the nucleosome core,

independently of H3K9me3 (KKVFS and KRQSRK)[38]. Consistently, Clr4 binding to
150 chromatin was increased in *ubc4-1* and *cul4-1* mutants, especially at *dh* centromeric repeats and at the *ade6*$^{+}$ reporter gene, where sRNAs are over-produced (Fig. 2a and Extended Data Figs. 5a,b and 7a). This increased binding of Clr4 to chromatin is not dependent on its chromodomain because there was no change in combination with a chromodomain mutant (*clr4-W31G ubc4*-1, Fig. 2a and Extended Data Fig. 5a)[18,40].
155 Mutating all lysines (*AllKtoR*) resulted in an even stronger affinity of Clr4 to chromatin (Fig. 2a). In contrast, Flag-Clr4 binding to centromeric heterochromatin decreased when H3K9me2/3 was completely abolished by *rik1Δ*, *raf1Δ* and *raf2Δ* (Fig. 2b)[26]**.** Clr4 also binds centromeric ncRNA[41] and this activity was strongly increased in *ubc4-1* and *cul4-1* mutants (Fig. 2c) indicating that both chromatin and ncRNA binding activities of Clr4 are
160 down regulated by Clr4 mono-ubiquitination.

To further explore the effect of Clr4 mono-ubiquitination on chromatin binding, we carried out nucleosome binding assays using *in vitro* ubiquitinated 6xHis-Clr4 recombinant protein and 3xFlag-Clr4 purified from *S. pombe* cells, with nucleosomes with either unmodified histone H3 (me0) or H3K9me3 (me3) tethered to streptavidin
165 beads. In contrast to unmodified Clr4 protein, which had strong binding affinity to the nucleosome, ubiquitinated Clr4 did not bind to nucleosomes (Fig. 2d and Extended Data Fig. 5c). These results suggest that Clr4 mono-ubiquitination promotes dissociation of Clr4 from chromatin in agreement with the *in vivo* Clr4 ChIP-seq data.

Next, we tested whether Ubc4-Cul4 ubiquitination activities are important *in vivo*
170 in the context of a minimal silencing system, relying on tethering Clr4 to a specific

chromatin locus. To do this, we generated a reporter system in which *clr4-ΔCD* lacking the chromodomain is fused to Gal4 DNA binding domain (GBD) and tethered to 5 Gal4-binding sites (5xUAS) upstream of *ade6*$^{+}$, inserted at the endogenous *ura4* locus, and with additional intact WT *clr4*$^{+}$ available[42]. Artificial tethering of GBD-*Clr4-ΔCD* resulted in silencing of the *ade6*$^{+}$ reporter gene as indicated by red colony formation on low-adenine medium and accumulation of H3K9me2/3 by ChIP-qPCR (Fig. 2e), in accordance with previous studies[42-47]. In contrast, *ade6*$^{+}$ silencing was greatly decreased by introduction of *ubc4-1* and *cul4-1* mutations, demonstrating that the ubiquitination activity of Ubc4-CLRC is required for spreading of silencing into the *ade6*$^{+}$ reporter (Fig. 2e).

Liquid-liquid phase separation (LLPS) is the mechanism by which cellular granules, including membraneless organelles such as the nucleolus, P granules, and stress granules form biomolecular condensates without a lipid bilayer. Multivalent macromolecular interactions, especially between proteins harboring intrinsically disordered regions (IDRs) and nucleic acids, drive formation of phase-separated liquid droplets. These biomolecular condensates have higher protein density and reduced internal diffusion, which contributes to a myriad of cellular functions, including heterochromatin formation[48-55]. Nucleosomes are post-translationally modified and many chromatin-related factors, such as heterochromatin protein 1 (HP1) and bromo-domain containing proteins (e.g. BRD4), which recognize these histone modifications, have an intrinsic propensity for LLPS and form phase-separated liquid droplets *in vitro* and in cells[56-60].

Like other HP1 proteins, *S. pombe* Swi6 has been shown to undergo liquid-liquid phase separation (LLPS) which contributes to the highly dynamic features of heterochromatin[57,59,61]. Clr4 and its mouse homolog, mSUV39H1, have an intrinsically disordered region (IDR), also known as a low-complexity domain (LCD), between its chromodomain (CD) and PreSET domain (Extended Data Fig. 6a,b)[38], and IDR/LCD are typically responsible for phase separation[48,50,52,54,55,62]. We found that recombinant GFP-Clr4^{Full} and GFP-Clr4^{IDR} (51-220 amino acids of Clr4) proteins readily form phase-separated liquid droplets *in vitro* in a salt-dependent manner even without addition of crowding agents (Fig. 3a and Extended Data Fig. 6c)[63]. The formation of phase-separated liquid droplets by GFP-Clr4^{IDR} was reduced by adding 1,6-hexanediol, which dissolves liquid droplets by disrupting the hydrophobic interactions of protein-protein or protein-RNA (Extended Data Fig. 6d)[54,64]. Furthermore, photobleaching of entire liquid droplets of GFP-Clr4^{IDR} resulted in slow but steady recovery of fluorescence indicative of dynamic exchange of GFP-Clr4^{IDR} protein inside and outside of liquid droplets (Fig. 3b and Extended Data Fig. 6e)[48,56,60]. These results indicate that phase-separated liquid droplets of Clr4 are indeed formed by LLPS.

As the oligomerization of HP1 is important to form phase-separated liquid droplets as well as during chromatin compaction, and as SUV39H1 and SUV39H2 are also able to tether together to form dimers[57,59,65-67], we reasoned that Clr4 may self-associate to form phase-separated liquid droplets. To do this, we mixed recombinant GFP-Clr4 and mCherry-Clr4 and found that these proteins readily associate together to form phase-separated liquid droplets, supporting the idea of Clr4 self-association (Fig. 3c). CTGS

215 during G1/S phase of the cell cycle is accompanied by transcription of ncRNAs and accumulation of sRNAs and the interaction of RNA-binding proteins with RNA are important for LLPS[17,19,48,51]. To investigate the possible role of centromeric ncRNA in Clr4 LLPS, we added 120 nt, synthetic centromeric ncRNA to GFP-Clr4/mCherry-Clr4. Surprisingly, ncRNA inhibited phase-separated liquid droplet formation of Clr4 and
220 Clr4^{IDR} in a dosage dependent manner (Fig. 3c and Extended Data Fig. 6c), reminiscent of other IDR-containing proteins that interact with RNA[68-70]. We next examined Clr4 self-association via immunoprecipitation using recombinant Flag-Clr4 and Myc-Clr4 proteins in the presence or absence of ncRNA. The weak interaction of Flag-Clr4 with Myc-Clr4 in the absence of ncRNA is consistent with multivalent weak interactions that form
225 phase-separated liquid droplets (Fig. 3d). In contrast, by addition of ncRNA, Clr4 self-association was greatly increased with increasing concentration of ncRNA, indicating that Clr4 self-association induced by ncRNA actually inhibits its phase-separated liquid droplet formation (Fig. 3c,d). Furthermore, mono-ubiquitinated Clr4 did not bind to the centromeric ncRNA compared to unmodified Clr4 protein from ncRNA binding assays
230 using 3xFlag-Clr4 purified from *S. pombe* cells (Extended Data Fig. 6f). Thus, the RNA binding activity of Clr4 is key for its dimerization and LLPS activities, and is inhibited by mono-ubiquitination.

Previously, ncRNA has been shown to inhibit Clr4 enzyme activity[38], but as nucleosomes were used as substrate, this was thought to be due to competition with
235 nucleosome binding. To characterize the effect of ncRNA-mediated dimerization on Clr4 H3K9 methylation activity, we fused the N terminal tail of *S. pombe* H3 (A1-K36) with

GST (H3N-GST) and used it as a substrate of Clr4 in the absence or presence of ncRNA[71]. Interestingly, Clr4 enzymatic activity for H3K9me3 decreased greatly as the concentration of ncRNA increases, while Clr4 enzymatic activity for H3K9me2 did not change with increasing ncRNA and dimerization of Clr4 (Fig. 3d,e). These results indicate that ncRNA binding and Clr4 dimerization has an inhibitory effect on Clr4 enzymatic activity for H3K9me3, independent of nucleosome binding.

SUV39H1 forms a complex with HP1, and SUV39H1 and HP1 together colocalize to distinct heterochromatic subnuclear domains (chromocenters) in human cells[60,67,72,73]. HP1α readily forms phase-separated liquid droplets without addition of DNA or nucleosomes *in vitro*, but HP1β only forms liquid droplets with addition of the N-terminal chromo domain (CD) of SUV39H1 and nucleosomes modified on histone H3K9me3[60]. *S. pombe* Swi6 forms phase-separated liquid droplets only in combination with nucleosomes[61]. Similarly, we found that recombinant mCherry-Swi6 alone could not form phase-separated liquid droplets *in vitro*. However, GFP-Clr4^{IDR} and mCherry-Swi6 could form phase-separated liquid droplets when mixed together (Fig. 3f). These droplets dissolved upon the addition of a much smaller amount of ncRNA compared to that required to dissolve droplets formed by mixing GFP-Clr4 with mCherry-Clr4 (Fig. 3f). Thus, phase-separated liquid droplet formation of Swi6 can be promoted by Clr4 independently of modified nucleosomes, but only during transcriptional silencing when RNA is absent. GFP-Swi6 localizes to heterochromatin *in vivo* in a H3K9me-dependent manner and we used this to assess heterochromatin condensation in *ubc4* mutant backgrounds (Fig. 3g). Compared to WT and *dcr1Δ* strains which have up to 4

condensed foci representing the centromeric chromocenter, telomere clusters and the
260 mating type locus, *ubc4-1* mutants retained only one visible chromocenter, presumably due to the complete loss of H3K9me2/3 and Swi6 at telomeres and mating-type loci detected by ChIP (Extended Data Fig. 2a-d). The remaining GFP-Swi6 foci were abolished in *dcr1Δ ubc4*-1, *ubc4-3xHA*, *cul4Δ* and *clr4Δ* mutants in accordance with complete loss of H3K9me2/3 from all heterochromatin in these mutants (Fig. 3g). These
265 results indicate that Swi6 forms condensates *in vitro* and *in vivo*, and that they are promoted by Clr4 in the absence of RNA during the G2 phase of the cell cycle. After mitosis, phosphorylation of H3S10 evicts Swi6 from heterochromatin, resulting in transient transcription in G1 and S phase[19]. RNA promotes self-association of Clr4 and rapid dissolution of heterochromatic condensates, consistent with previously observed
270 de-clustering of GFP-Swi6 chromocenters[74]. Subsequent mono-ubiquitination by CLRC releases Clr4 from RNA and promotes LLPS together with H3K9me3 and Swi6 to drive the transition to TGS in G2.

It has recently been shown that Ubc4 and Cul4 are strongly enriched in Swi6-associated chromatin, along with other CLRC subunits, as well as in chromatin
275 associated with the BET family double bromodomain protein Bdf2 (a homolog of mammalian BRD4)[36]. Bdf2 is recruited by the putative H3K9 demethylase, Epe1, which localizes to centromeric heterochromatin in a Swi6-dependent manner and contributes to sRNA production[75-77], which also occurs mainly in S phase[19]. Bdf2 binds to RNA Pol II promoters at the centromeric heterochromatin boundary[78] and interacts with the TFIID
280 transcription factor complex[79,80] while Epe1 is confined to these boundaries by Cul4-

Ddb1^{Cdt2} E3 ligase-dependent poly-ubiquitination[75]. We found that the increased centromeric sRNA production in *ubc4-1* and *cul4-1* mutants was accompanied by spreading of Epe1 and Bdf2 to pericentromeric repeats, as well as Ago1 and Chp1, two components of the RITS siRNA complex (Figs. 1f and 4a,b and Extended Data Fig. 7a-c). Moreover, *epe1Δ* and *bdf2Δ* deletion mutants suppressed the increased sRNA production in *ubc4-1* and *cul4-1* mutants back to wild-type levels (Fig. 4a), by reducing recruitment of RNA Pol II (Extended Data Fig. 7d). Consistent with the regulation of Epe1 by Cul4[75], we found that Ubc4 and CLRC induced poly-ubiquitination and degradation of Bdf2 (Fig. 4c and Extended Data Fig. 7e,f). Bdf2^{BRD4} recruits TFIID and RNA Pol II to centromeric heterochromatin, an important step in precursor ncRNA transcription for sRNA production[79,80]. To mimic the effect of *ubc4-1* and *cul4-1* on sRNA production, we overexpressed Epe1 (*epe1-OE*, Extended Data Fig. 7g). As expected, *epe1-OE* resulted in increased sRNA production by increased recruitment of Epe1 and Bdf2, but unlike *ubc4-1* and *cul4-1*, it also resulted in decrease of both H3K9me2 and H3K9me3 at centromeric heterochromatin (Fig. 4a,b and Extended Data Fig. 7h-j). Thus, Ubc4-CLRC regulates sRNA production separately through Epe1 and Bdf2, which in combination with Clr4, regulates the proper transition from CTGS to TGS (Extended Data Fig. 7k).

Ubiquitination is a reversible, highly dynamic and transient modification, and its removal is catalyzed by deubiquitinating enzymes[21,81,82]. A deletion mutant of the deubiquitinating enzyme Ubp3 rescues the heterochromatic silencing defects of *ago1Δ,* and *ubp3Δ* shows positive epistatic genetic interactions with CLRC component

mutants[83,84]. While deletion of Ubp3 did not increase Clr4 mono-ubiquitination most likely because of redundancy between de-ubiquitinating enzymes (Extended Data Fig. 8a)[85], the overexpression of Ubp3 (*ubp3-OE*) resulted in a silencing defect at the centromeric *ura4*$^{+}$ reporter gene and reduced mono-ubiquitination of Clr4, supporting the idea that Ubp3 counteracts Clr4 mono-ubiquitination by Ubc4-CLRC (Fig. 4d and Extended Data Fig. 8b,c). The overexpression of Ubp3 also resulted in an increase of H3K9me2 and decrease of H3K9me3, as well as increased sRNA production, with increased binding of Epe1 and Bdf2 to centromeric heterochromatin, resembling the phenotypes of *ubc4-1* or *cul4-1* mutants at centromeric heterochromatin (Fig. 4e and Extended Data Fig. 8d). Similarly, at telomeres, *ubp3-OE* resulted in increased H3K9me2 but decreased H3K9me3 as well as greatly increased recruitment of Epe1 and Bdf2, resulting in ectopic sRNA production (Fig. 4e, right and Extended Data Fig. 8e). The 5'-nucleotide of these sRNAs from centromere and subtelomere repeats had a strong U/A bias and the typical sRNA size was 23±1 nt, as is expected for *bona fide* RNAi products (Fig. 4f,g)[12,86]. These results indicate that Ubp3 counteracts the activities of Ubc4-CLRC, both in terms of H3K9me2/3 transitions and sRNA production, with overexpression of Ubp3, making the chromatin structure of telomeres resemble that of the centromere.

Our findings indicate that, while CTGS and H3K9 di-methylation depend strictly on RNAi, mono-ubiquitination of Clr4 promotes the transition from CTGS to TGS by first releasing Clr4 from heterochromatin. The key lysine residues in the IDR form a β-sheet on binding of the nucleosome core[38], which is likely disrupted by ubiquitination.

325 Deubiquitination by Ubp3 then allows re-engagement and spreading of H3K9 tri-methylation to adjacent chromatin, as demonstrated by ectopic heterochromatin formation at the *ade6*$^{+}$ reporter gene mediated by tethered Clr4 (Fig. 2e). Spreading plays a similar role at the silent mating type locus and at telomeres where heterochromatic silencing is completely lost in *ubc4-1* and *cul4-1* mutants (Extended
330 Data Figs. 1d and 2b,c). The ability to induce the spreading of silencing by this mechanism may be critical at these genomic loci as these chromosomal locations have only limited capacity for ncRNA transcription and RNAi.

Ubc4-CLRC likely has additional functions, such as H3K14 ubiquitination, which was recently shown to enhance H3K9 methylation *in vitro*[71]. But H3K9me2 and
335 H3K9me3 are both lost at centromeres in H3K14R mutants, which suggests that H3K14 ubiquitination is essential for histone H3K9 methylation but not for transition of H3K9me2 to H3K9me3 (Extended Data Fig. 9a-c). Centromeric sRNA production was not affected by mutants in the chromo- (*clr4-W31G*), and SET domains (-*F449Y* and -*I418P*) which are also defective in the H3K9me2-to-H3K9me3 transition (Extended
340 Data Fig. 9d,e)[18]. Interestingly, we found that *clr4-W31G*, -*F449Y* and -*I418P* mutants also have reduced Clr4 mono-ubiquitination indicating a strong correlation between Clr4 mono-ubiquitination and transition of H3K9me2 to me3 (Extended Data Fig. 9f,g). Recently, phosphorylation of the Clr4 SET domain by Cdk1 was also shown to be required for H3K9me3 during meiosis, and for proper gametogenesis, although the role
345 in silencing, if any, was not examined[87]. The hierarchical relationship between phosphorylation, auto-methylation and mono-ubiquitination of Clr4 remains to be

explored[39].

Like Swi6, Clr4 undergoes strong, spontaneous LLPS to form biomolecular condensates and this property is mediated by the IDR. Post-translational modifications of IDRs, and their association with RNA, can affect protein function significantly; including the induction of disorder-to-order transitions, alternative complex formation and differential subcellular localization[88-94]. We found that ubiquitination of the IDR of Clr4 prevents RNA binding and protein dimerization. This promotes LLPS, and is critical for the CTGS to TGS transition. These phase-separated liquid droplets of Clr4 and Clr4/Swi6 are rapidly dissolved in the presence of ncRNA and this RNA-dependent interaction promotes Clr4 dimerization instead (Fig. 3c,d,f and Extended Data Fig. 6c). Intriguingly, binding of centromeric ncRNA to the Swi6 hinge region, which is also disordered and lysine-rich, has previously been shown to prevent Swi6 binding to chromatin[95], consistent with our results. In the absence of mono-ubiquitination, Clr4 recruitment to genomic loci where ncRNA and sRNA are overproduced greatly increased in agreement with previous studies that mammalian SUV39H1 chromodomain binds to pericentromeric RNA for the recruitment of SUV39H1 to heterochromatin, H3K9me3 deposition and heterochromatin assembly (Fig. 2a, c)[96-98]. We found that ncRNA binding inhibits Clr4 enzymatic activity for H3K9me3 likely through binding of ncRNA to the chromodomain and IDR of Clr4 and subsequent dimerization (Fig. 3d, e and Extended Data Fig. 6a, c)[41].

In summary (Extended Data Fig. 10), we have found that ncRNA transcription and sRNA production during G1/S promote CTGS and H3K9 di-methylation through

recruitment of CLRC. The production of sRNA depends on the transcriptional co-
370 activator Epe1-Bdf2, which licenses recruitment of RNA Pol II to transcriptionally permissive heterochromatin[13-15,18,33,40,46,99,100]. Subsequently, removal of Epe1-Bdf2 by Ubc4-CLRC-mediated poly-ubiquitination silences transcription, while Clr4 mono-ubiquitination is required for its dissociation from chromatin, and from ncRNA, triggering Clr4 dependent H3K9me3 and phase separation of Clr4 along with Swi6. De-
375 ubiquitination of Clr4 by Ubp3 promotes additional modification and spreading of H3K9me3 to nearby nucleosomes and subsequent binding of HP1 proteins, Swi6 and Chp2 important for RNAi-independent TGS[18,40,101]. Removal of ubiquitin moieties from Epe1-Bdf2 allows rapid recycling of these factors for the next cell cycle. In the absence of RNAi, variable amounts of H3K9me2 are maintained at the centromere, indicating
380 that Clr4 must be recruited, at least in part independently of RNAi[102]. Based on our results, one explanation is that ncRNA, in the presence of existing H3K9 methylation, initially recruits Clr4 and promotes dimerization and chromatin binding. Subsequently, RNAi recruits the Ubc4-Cul4-Rik1^{Raf1Raf2} E3 ligase[46], which mono-ubiquitinates Clr4 preventing RNA binding, and promoting H3K9me3, phase separation and spreading
385 along with other phase separated chromatin proteins, such as Swi6 (Extended Data Fig. 10). Given the high conservation of Ubc4, Clr4, Brd4 and Cul4, similar transitions between RNAi-dependent gene silencing and heterochromatin assembly may be regulated by ubiquitination and RNA in other organisms, including mammals, where TRIM28, HP1 and SUVH39 form condensates with H3K9me3 nucleosome arrays,
390 similar to those reported here[60].

Acknowledgement

We thank all Martienssen lab members for valuable discussions and suggestions. The authors acknowledge assistance from the Cold Spring Harbor Laboratory Shared Resources, which are funded in part by the Cancer Center Support Grant (5PP30CA045508). This work was supported by the Howard Hughes Medical Institute, and a grant from the National Institute of Health (R35GM144206) (to R.A.M.).

Author contributions

H.S.K. performed experiments and bioinformatics. B.R. contributed sRNA-seq experiments and bioinformatics. A.Y.C. contributed to EMS mutagenesis, C.H. contributed to LLPS. S.B. LT and AV contributed to protein purification. H.S.K. and R.A.M. designed the experiments and wrote the manuscript.

Declaration of interests

The authors declare no competing interests.

Data availability

Genome-wide datasets are deposited in the Gene Expression Omnibus (GEO) under the accession number GSE156069.

Materials and Method

Yeast strains and plasmids manipulation

Yeast strains, plasmids, oligonucleotide sequences and antibodies are listed in
410 Supplemental Tables S1-S4. All yeast strains were constructed by the PCR-based targeting method[103] and lithium-acetate transformation method[104]. For N-terminus tagging of 3xFlag to *clr4*, *rik1* and *raf1*, endogenous promoters and terminators of each gene were used. For C-terminus tagging of 3xFlag, 3xFlag sequence and *adh1* terminator with Kan resistant (Kan^R) gene was inserted at the end of open reading
415 frames (ORF). For some 3xFlag-Clr4 lysine mutants, *adh1* terminator with Kan resistant (Kan^R) gene was inserted at the end of *clr4* open reading frames (ORF). For overexpression of *ubp3*, *ubp8*, and *epe1*, 500 bp of *adh1* promoter was inserted between their promoter and ORF. To construct pET-14b-Clr4, the coding DNA sequence of full-length Clr4 (amino acids 1-490) was amplified from *S. pombe* genomic
420 DNA, digested with *NdeI* and cloned into *NdeI*-digested pET-14b. For pHis-parallel-GFP-$Clr4^{Full}$ and pHis-parallel-GFP-$Clr4^{IDR}$ construction, the coding DNA sequence of full-length $Clr4^{Full}$ (amino acids 1-490) and $Clr4^{IDR}$ (amino acids 51-220) were amplified from *S. pombe* genomic DNA, digested with *BamHI*/*XhoI* and cloned into *BamHI*/*XhoI*-digested pHis-parallel-GFP. For pHis-parallel-mCherry-Clr4, mCherry-Clr4 DNA
425 sequence was synthesized (IDT), digested with *NdeI*/*XhoI* and cloned into *NdeI*/*XhoI*-digested pHis-parallel-GFP. For pHis-$Clr4^{IDR}$-GFP, DNA sequence was synthesized (IDT) and cloned into pET-14b vector using In-Fusion HD cloning kit (Takara). To construct pET-14b-Flag-Clr4 and pET-14b-Myc-Clr4, the coding DNA sequence of full-

length Clr4 (amino acids 1-490) was amplified from *S. pombe* genomic DNA using
430 oligomers containing 6xHis-1xFlag or 6xHis-1xMyc sequences respectively and cloned into pET-14b vector using In-Fusion HD cloning kit (Takara).

Silencing spot assay

Cells grown freshly on YES plate were picked and resuspended in water to make a
435 concentration of ~5 × 10^4 cells per µl. 8 µl of 10-fold serial dilutions were spotted on appropriate plates like YES, low adenine (Low Ade), EMM-Ura (-Ura), and YES+TBZ (TBZ), and incubated 3 days at 30 °C for photography. *ura4*$^+$ reporter gene silencing was also tested on 5-fluoro-orotic acid (FOA) plates, which kills cells expressing Ura4.

440 **Iodine staining**

Freshly grown yeast cells were spotted on SPA plates to induce sporulation, incubated at room temperature for 3 days, and then stained with iodine vapor for 2-3 min. Staining of starch which is abundant in mature spore produces a dark brown color.

445 **EMS mutagenesis and whole-genome sequencing for *ubc4-G48D suppressor***

EMS mutagenesis was carried out as previously described[105]. Briefly, freshly grown 1 x 10^9 yeast cells were washed with distilled water, resuspended in 1.5 ml of 0.1 M sodium phosphate buffer (pH 7.0) and treated with 50 µl EMS (Sigma M0880) for 1h at 30 °C. 0.2 ml of treated cells was moved to 8 ml of sterile 5% sodium thiosulfate to inactivate
450 EMS. Cells were washed, resuspended in sterile water and plated on YES plate. Single

colonies from plates were patched on SPA plates to induce sporulation, incubated at room temperature for 3 days, and then stained with iodine vapor for 2-3 min. For whole-genome sequencing for *ubc4-G48D* suppressors, genomic DNA was purified from freshly grown yeast cells using Genomic-tip 20/G column (QIAGEN 10223). DNA library was constructed using the TruSeq DNA PCR-Free Library Prep Kit (Illumina 20015962). Barcoded DNA library was sequenced using Illumina MiSeq platform, which generates paired-end 151 nt reads and analyzed as previously described [106]. Briefly, reads were adapter-trimmed and quality-filtered using Sickle (paired-end mode), then mapped to the *S. pombe* genome using Bowtie2[107]. Duplicate reads were removed using Samtools (≤ 0.14% per library). SNPs were called using FreeBayes to find SNPs present in suppressor strain but absent in the parental strain[108]. This uncovered a G→C transversion at position chr2:716,192, a second-site mutation in the *ubc4* gene. The mutation was verified by Sanger sequencing and confirmed to be causative by constructing the same fresh mutation in WT and *ubc4-1* strains.

Live cell imaging

Images of freshly growing cells were collected using Zeiss Axio Imager M2 with DIC and EGFP channels and processed using Zeiss Zen software.

Quantitative reverse transcription PCR (RT-qPCR)

Total RNAs were purified from freshly grown yeast cells using *Quick*-RNA Fungal/Bacterial Miniprep Kit (Zymoresearch R2014). Genomic DNAs were removed

using DNase I (Roche 04716728001) and RNAs were cleaned using RNA Clean & Concentrator (Zymoresearch R1013). Reverse transcription was carried out using SuperScript IV First-Strand Synthesis System (ThermoFisher 18091050) with random hexamer or oligo dT as primers. For quantitative PCR (qPCR), iQ SYBR Green Supermix (Bio-rad 1708882) was used with the primers listed in Supplemental Table S3 and samples were run on CFX96 Real-Time PCR Detection System (Bio-rad).

Chromatin Immunoprecipitation (ChIP)

Chromatin Immunoprecipitation (ChIP) experiments were performed as previously described[79]. Briefly, freshly grown 40 ml cells in YES were fixed with 1% formaldehyde from 37% stock (Sigma F8775) for 20 min at room temperature for H3K9me2, H3K9me3, RNA Pol II, Ago1 and Chp1 ChIP. For Swi6 and 3xFlag-Clr4 ChIP, 40 ml cells were pre-incubated at 18 °C for 2 h and fixed with 1.45% Formaldehyde from 16% stock (ThermoFisher 28908) for 30 min at 18 °C. Cells were quenched with 360 mM glycine and 2.4 mM Tris for 5 min. Whole-cell extracts (WCE) were prepared using FastPrep-24 and sonicated using Covaris. 1~2 µg of antibodies like anti-H3K9me2 (Abcam ab1220), anti-H3K9me3 (Absolute Antibody Ab00700-1.26), anti-RNA polymerase II (BioLegend 904001), Swi6 (Abcam ab188276), Ago1 (Abcam Ab18190), Chp1 (Abcam ab18191) and anti-Flag (Sigma F1804) were pre-incubated with 50 µl Protein A and Protein G sepharose (GE 17513801 and 17061801) mix for 3~4 h and then incubated with sheared chromatin overnight at 4 °C. After washing, bead-antibody-chromatin mixture were treated with Proteinase K (ThermoFisher 100005393) for 1 h at

495 42 °C and incubated 5~6 h at 65 °C to reverse cross-links. DNA was cleaned up using ChIP DNA Clean & Concentrator (Zymo Research D5205) and subsequently used for qPCR or ChIP-Seq.

ChIP-seq

500 ChIP-Seq libraries were constructed using NEBNext Ultra II DNA Library Prep Kit for Illumina (NEB E7645) and barcoded multiplex libraries were sequenced using Illumina MiSeq platform, which generates paired-end 101 bp reads. Raw reads were trimmed using Trimmomatic, mapped to *S. pombe* genome using Bowtie2 and visualized in IGV genome browser. Total ChIP-seq read counts for defined region were analyzed using
505 MultiBigwigSummary or MultiBamSummary.

sRNA-seq

For sRNA-seq, total RNAs were purified from freshly grown yeast cells using *Quick*-RNA Fungal/Bacterial Miniprep Kit (Zymoresearch R2014) and sRNA were enriched
510 using RNA Clean & Concentrator (Zymoresearch R1013). sRNA libraries were constructed using NEBNext Small RNA Library Prep Set for Illumina (NEB E7330) and barcoded multiplex libraries were sequenced using Illumina MiSeq platform, which generates single-end 36 nt reads. Reads were adapter-trimmed using Cutadapt se, keeping a minimum read size of 15 nt, and mapped to the *S. pombe* genome using
515 Bowtie[109] allowing up to 1 mismatch. The strand-specific genomic coverage was calculated using Bedtools[110].

Co-Immunoprecipitation (Co-IP) and Western blotting (WB)

Whole-cell extracts (WCE) were prepared from freshly grown yeast cells in lysis buffer
520 (40mM Tris-HCl, pH 7.5, 1 mM EDTA, 10% Glycerol, 0.1% NP-40, 300 mM NaCl) with Protease inhibitor cocktail (Roche 11836170001). For Co-IP of Cul4-GFP with Ubc4, 2 µg of GFP antibody (Roche 11814460001) was pre-incubated with 50 µl Protein A and Protein G Sepharose (GE Healthcare 17513801 and 17061801) mix for 3~4 h and then incubated with WCE overnight at 4 °C. After washing, purified proteins were boiled and
525 loaded on 4–20% Mini-PROTEAN TGX Gel (Bio-rad 456-1093) and Western blotting was performed with anti-GFP (Abcam 290) and anti-mUBE2D3 (Proteintech 11677-1-AP) antibodies to detect Cul4-GFP and Ubc4 using ECL (Thermo Fisher 32209) assay according to the manufacturer's instruction. For Co-IP of Flag-Rik1, Flag-Dos1 or Dos2-Flag with Ubc4, 50 µl of Anti-Flag M2 Affinity Gel (Sigma A2220) was incubated with
530 WCE overnight at 4 °C. For detection of Flag tagged protein and Ubc4, anti-Flag (Sigma F7425) and anti-mUBE2D3 (Proteintech 11677-1-AP) antibodies were used.

Purification of ubiquitinated Flag-Clr4 and Bdf2-Flag proteins

For purification of ubiquitinated Flag-Clr4, WCE prepared from freshly grown cells in
535 lysis buffer (50mM Hepes, pH 7.6, 150mM NaCl, 300mM KAc, 5mM MgAc, 10% Glycerol, 20mM β-GP, 1mM EDTA, 1mM EGTA, 0.1% NP-40, 1mM DTT, 250U/ml Dnase I (Roche 04716728001), 25~50 µg/ml Rnase A (Sigma R4642), 1mM PMSF, 0.3mM PR-619 (Sigma 662141)) with Protease inhibitor cocktail (Roche 11836170001)

and De-ubiquitination/sumoylation Inhibitor (Cytoskeleton NEM09BB) was incubated
540 with Anti-Flag M2 Affinity Gel or Ubiquitination Affinity Beads (UAB, Cytoskeleton UBA01- Beads) overnight at 4 °C. After washing, purified proteins were loaded on 4–20% Mini-PROTEAN TGX Gel (Bio-rad 456-1093). For detection of ubiquitinated Clr4 protein, anti-Flag (Sigma F7425) or anti-ubiquitin (Cell Signalling 3936T) antibodies were used. Cells were also treated with proteasome inhibitor 100 µM MG-132
545 (APExBIO A2585) for 4 h before harvesting to detect poly-ubiquitinated Bdf2-Flag or to see the effect of blocking proteasome pathway by treating MG-132 on mono-ubiquitinated Flag-Clr4.

CLRC complex purification from *S. pombe*

550 Protein purifications were performed as described previously[15]. Briefly, Rik1-TAP were purified from 6 to 12 g of cells. Cells were lysed in 1 volume of lysis buffer (50 mM HEPES-KOH, pH 7.6, 300 mM KAc, 10% glycerol, 1 mM EGTA, 1 mM EDTA, 0.1% NP-40, 1 mM DTT, 5 mM MgAc, 1 mM NaF, 20 mM β-GP, 1 mM PMSF, 1 mM Benzamidine and 1 µg/ml of Leupeptin, Aprotinin, Bestatin and Pepstatin). 1 volume lysis buffer was
555 added and the lysate was centrifuged at 16,500 rpm for 25 min at 4 °C in a SA600 rotor. The first affinity purification was performed using Ig-G Sepharose beads at 4 °C for 2 h. The beads were washed with lysis buffer and TEV-C buffer (10 mM Tris-HCl, pH 8.0, 150 mM KAc, 0.1% NP-40, 0.5 mM EDTA, 1 mM DTT) and bound protein was eluted using a GST-TEV protease. The eluate was diluted in 2 volumes of CAM-B buffer (10
560 mM Tris-HCL, pH 8.0, 150 mM NaCl, 1 mM MgAc, 1 mM Imidazole, 2 mM $CaCl_2$, 10

mM βME) and the second affinity purification was performed by adding Calmodulin-Sepharose at 4 °C for 1 h. The beads lysate was washed with CAM-B buffer containing 0.1 % NP-40 and bound protein was eluted with CAM-E buffer (10 mM Tris-HCL, pH 8.0, 150 mM NaCl, 1 mM MgAc, 1 mM Imidazole, 10 mM EGTA, 10 mM βME). Purified CLRC complex was added to *in vitro* ubiquitination assay of 6xHis-Clr4.

Recombinant protein purification from *E. coli*, *in vitro* ubiquitination and nucleosome binding assay

BL21-CodonPlus (DE3)-RIL strains (Agilent Technologies 230245) that express recombinant Clr4 proteins were grown with 0.4 mM IPTG for 20 h at 18 °C. Induced proteins were purified on HisPur Ni-NTA Superflow Agarose (ThermoFisher 25214) and eluted with elution buffer containing 150 mM Imidazole. The recombinant proteins purified from *E. coli* were further dialyzed against 1x TBS using Slide-A-Lyzer Dialysis Cassettes (ThermoFisher 66003). For *in vitro* ubiquitination, recombinant 6xHis-Clr4 protein or 3xFlag-Clr4 purified form *S. pombe* cells were mixed with human Ubiquitin-activating Enzyme (UBE1, R&D systems E-305), human UbcH5c/UBE2D3 (R&D systems E2-627), human Ubiquitin (R&D systems U-100H) or human HA-Ubiquitin (R&D systems U-110), Mg-ATP (R&D systems B-20) and 10x E3 Ligase Reaction Buffer (R&D systems B-71) with or without CLRC complex purified from *S. pombe* cells. For nucleosome or ncRNA binding assay, biotin labeled Recombinant Mononucleosomes (H3.1, Active Motif 31467) and Recombinant Mononucleosomes H3K9me3 (H3.2, Active Motif 31555) or biotin labeled ncRNA (synthesized from IDT)

were pre-incubated with Streptavidin beads (GE Healthcare 17-5113-01) and incubated *in vitro* ubiquitinated 6xHis-Clr4 or Flag-Clr4 proteins purified from *S. pombe* cells.
585 Samples were washed, boiled and loaded on 4–20% Mini-PROTEAN TGX Gel (Bio-rad 456-1093) and WB was performed with anti-Flag (Abcam ab1791), anti-H3K9me3 (Abcam ab8898) and anti-H3 (Abcam ab1791), and using ECL (Thermo Fisher 32209) assay according to the manufacturer's instruction.

590 **Mass Spectrometry**

The gel band sample was reduced and alkylated with *N*-ethylmaleimide (NEM), digested with trypsin for 1.5 h at 37 °C and washed with ammonium bicarbonate/acetonitrile to remove stain, SDS and other reagents. Peptides were extracted from the gel pieces, dried down and re-dissolved in 2.5% acetonitrile, 0.1%
595 formic acid. Each digest was run by nanoLC-MS/MS using a 2 h gradient on a 0.075 mm x 250 mm C18 column feeding into a Q-Exactive HF mass spectrometer. All MS/MS samples were analyzed using Mascot (Matrix Science, London, UK; version 2.6.1). Mascot was set up to search the cRAP_20150130.fasta; custom4_20190215.fasta; SwissProt_2019_02 database (selected for
600 *Schizosaccharomyces pombe*, unknown version, 5269 entries) assuming the digestion enzyme trypsin. Mascot was searched with a fragment ion mass tolerance of 0.060 Da and a parent ion tolerance of 10.0 PPM. Deamidated of asparagine and glutamine, oxidation of methionine, phospho of serine, threonine and tyrosine, GG of lysine, N-ethylmaleimide of cysteine were specified in Mascot as variable modifications. Scaffold

605 (version Scaffold_4.8.9, Proteome Software Inc., Portland, OR) was used to validate MS/MS based peptide and protein identifications. Peptide identifications were accepted if they could be established at greater than 80.0% probability by the Peptide Prophet algorithm[111] with Scaffold delta-mass correction. Protein identifications were accepted if they could be established at greater than 99.0% probability and contained at least 2
610 identified peptides. Protein probabilities were assigned by the Protein Prophet algorithm [112]. Proteins that contained similar peptides and could not be differentiated based on MS/MS analysis alone were grouped to satisfy the principles of parsimony. Proteins sharing significant peptide evidence were grouped into clusters.

615 **Liquid-Liquid Phase Separation (LLPS)**

LLPS of GFP-Clr4, mCherry-Clr4, GFP-Clr4^{IDR} and Clr4^{IDR}-GFP proteins were induced by diluting proteins to 100-500 nM range in 10 mM HEPES buffer (pH 7.6). To observe the effect of ncRNA on Clr4 LLPS, 120nt synthesized centromeric ncRNA (IDT) was added to the Clr4 proteins. To observe the effect of 1,6-Hexanediol (Sigma H11807) on
620 GFP-Clr4^{IDR} LLPS, GFP-Clr4^{IDR} protein was diluted to 10 mM HEPES buffers (pH 7.6) containing 5% Ethanol or 5% Hexanediol. LLPS was imaged on Zeiss Axio Imager M2 with differential interference contrast (DIC) and EGFP channels and processed using Zeiss Zen software.

625 **Fluorescence Recovery After Photobleaching (FRAP) experiments**

FRAP experiments were performed as previously described[113]. Briefly, 500 nM of GFP-

Clr4^{IDR} protein were diluted in 3.6% PEG8000. PEG8000 was used to stabilize phase-separated liquid droplets during the experiments. FRAP experiments were carried out using Zeiss LSM710 Confocal Laser Scanning Microscope with 63x objective. All
630 Bleaching experiments were performed with 488 nm argon laser at 100% intensity. Images before and after photobleaching were taken at 5 s interval and analyzed using standard methods.

***In vitro* pull down assay**

635 4 µg of Flag antibody (Sigma F1804) was pre-incubated with 50 µl Protein A and Protein G Sepharose (GE Healthcare 17513801 and 17061801) mix in 1 mL lysis buffer (40mM Tris-HCl, pH 7.5, 1 mM EDTA, 10% Glycerol, 0.1% NP-40, 250 mM NaCl) for 1 hr and then incunbated with recombinant Flag-Clr4 and Myc-Clr4 proteins (500 nM each) and different amount of ncRNA (0, 50, 100 and 200 nM) in 500 µL lysis buffer at
640 4 °C for 3 hr. After washing, purified proteins were boiled and loaded on 4–20% Mini-PROTEAN TGX Gel (Bio-rad 456-1093) and Western blotting was performed with anti-Myc (Abcam ab9106), and anti-Flag (Sigma, F7425) using ECL (Thermo Fisher 32209) assay according to the manufacturer's instruction.

645 ***In vitro* histone methylation (HMT) assay**

Recombinant Flag-Clr4 protein (5 µM) were mixed with recombinant H3N-GST (10 µM), 200 µM *S*-(5′-Adenosyl)-*L*-methionine chloride dihydrochloride (SAM, Sigma 7007) and different amoount of ncRNA (0, 0.5, 1 and 2 µM) in 50 µL HMT buffer (50mM Tris, pH

8.0, 20 mM KCl, 10 mM $MgCl_2$, 5% Glycerol, 1 mM DTT and 1 mM PMSF) and incubated at 30 °C for 1.25 hr. Samples were boiled and loaded on 4–20% Mini-PROTEAN TGX Gel (Bio-rad 456-1093) and Western blotting was performed with anti-H3K9me2 (Abcam ab1220), and anti-H3K9me3 (Absolute Antibody Ab00700-1.26) using ECL (Thermo Fisher 32209) assay according to the manufacturer's instruction.

References

1 Castel, S. E. & Martienssen, R. A. RNA interference in the nucleus: roles for small RNAs in transcription, epigenetics and beyond. *Nat Rev Genet* **14**, 100-112, doi:10.1038/nrg3355 (2013).

2 Janssen, A., Colmenares, S. U. & Karpen, G. H. Heterochromatin: Guardian of the Genome. *Annu Rev Cell Dev Biol* **34**, 265-288, doi:10.1146/annurev-cellbio-100617-062653 (2018).

3 Allshire, R. C. & Madhani, H. D. Ten principles of heterochromatin formation and function. *Nat Rev Mol Cell Biol* **19**, 229-244, doi:10.1038/nrm.2017.119 (2018).

4 Martienssen, R. & Moazed, D. RNAi and heterochromatin assembly. *Cold Spring Harb Perspect Biol* **7**, a019323, doi:10.1101/cshperspect.a019323 (2015).

5 Gutbrod, M. J. *et al.* Dicer promotes genome stability via the bromodomain transcriptional co-activator BRD4. *Nat Commun* **13**, 1001, doi:10.1038/s41467-022-28554-8 (2022).

6 Hall, I. M., Noma, K. & Grewal, S. I. RNA interference machinery regulates chromosome dynamics during mitosis and meiosis in fission yeast. *Proc Natl Acad Sci U S A* **100**, 193-198, doi:10.1073/pnas.232688099 (2003).

7 Provost, P. *et al.* Dicer is required for chromosome segregation and gene silencing in fission yeast cells. *Proc Natl Acad Sci U S A* **99**, 16648-16653, doi:10.1073/pnas.212633199 (2002).

8 Bannister, A. J. *et al.* Selective recognition of methylated lysine 9 on histone H3 by the HP1 chromo domain. *Nature* **410**, 120-124, doi:10.1038/35065138 (2001).

9 Nakayama, J., Rice, J. C., Strahl, B. D., Allis, C. D. & Grewal, S. I. Role of histone H3 lysine 9 methylation in epigenetic control of heterochromatin assembly. *Science* **292**, 110-113, doi:10.1126/science.1060118 (2001).

10 Rea, S. *et al.* Regulation of chromatin structure by site-specific histone H3 methyltransferases. *Nature* **406**, 593-599, doi:10.1038/35020506 (2000).

11 Colmenares, S. U., Buker, S. M., Buhler, M., Dlakić, M. & Moazed, D. Coupling of double-stranded RNA synthesis and siRNA generation in fission yeast RNAi. *Mol Cell* **27**, 449-461, doi:10.1016/j.molcel.2007.07.007 (2007).

12 Djupedal, I. *et al.* Analysis of small RNA in fission yeast; centromeric siRNAs are potentially generated through a structured RNA. *Embo j* **28**, 3832-3844, doi:10.1038/emboj.2009.351 (2009).
13 Motamedi, M. R. *et al.* Two RNAi complexes, RITS and RDRC, physically interact and localize to noncoding centromeric RNAs. *Cell* **119**, 789-802, doi:10.1016/j.cell.2004.11.034 (2004).
14 Volpe, T. A. *et al.* Regulation of heterochromatic silencing and histone H3 lysine-9 methylation by RNAi. *Science* **297**, 1833-1837, doi:10.1126/science.1074973 (2002).
15 Verdel, A. *et al.* RNAi-mediated targeting of heterochromatin by the RITS complex. *Science* **303**, 672-676, doi:10.1126/science.1093686 (2004).
16 Gutbrod, M. J. & Martienssen, R. A. Conserved chromosomal functions of RNA interference. *Nat Rev Genet* **21**, 311-331, doi:10.1038/s41576-019-0203-6 (2020).
17 Chen, E. S. *et al.* Cell cycle control of centromeric repeat transcription and heterochromatin assembly. *Nature* **451**, 734-737, doi:10.1038/nature06561 (2008).
18 Jih, G. *et al.* Unique roles for histone H3K9me states in RNAi and heritable silencing of transcription. *Nature* **547**, 463-467, doi:10.1038/nature23267 (2017).
19 Kloc, A., Zaratiegui, M., Nora, E. & Martienssen, R. RNA interference guides histone modification during the S phase of chromosomal replication. *Curr Biol* **18**, 490-495, doi:10.1016/j.cub.2008.03.016 (2008).
20 Cappadocia, L. & Lima, C. D. Ubiquitin-like Protein Conjugation: Structures, Chemistry, and Mechanism. *Chem Rev* **118**, 889-918, doi:10.1021/acs.chemrev.6b00737 (2018).
21 Hochstrasser, M. Origin and function of ubiquitin-like proteins. *Nature* **458**, 422-429, doi:10.1038/nature07958 (2009).
22 Rape, M. Ubiquitylation at the crossroads of development and disease. *Nat Rev Mol Cell Biol* **19**, 59-70, doi:10.1038/nrm.2017.83 (2018).
23 Swatek, K. N. & Komander, D. Ubiquitin modifications. *Cell Res* **26**, 399-422, doi:10.1038/cr.2016.39 (2016).
24 Ye, Y. & Rape, M. Building ubiquitin chains: E2 enzymes at work. *Nat Rev Mol Cell Biol* **10**, 755-764, doi:10.1038/nrm2780 (2009).
25 Hong, E. J., Villén, J., Gerace, E. L., Gygi, S. P. & Moazed, D. A cullin E3 ubiquitin ligase complex associates with Rik1 and the Clr4 histone H3-K9 methyltransferase and is required for RNAi-mediated heterochromatin formation. *RNA Biol* **2**, 106-111, doi:10.4161/rna.2.3.2131 (2005).
26 Horn, P. J., Bastie, J. N. & Peterson, C. L. A Rik1-associated, cullin-dependent E3 ubiquitin ligase is essential for heterochromatin formation. *Genes Dev* **19**, 1705-1714, doi:10.1101/gad.1328005 (2005).
27 Jia, S., Kobayashi, R. & Grewal, S. I. Ubiquitin ligase component Cul4 associates with Clr4 histone methyltransferase to assemble heterochromatin. *Nat Cell Biol* **7**, 1007-1013, doi:10.1038/ncb1300 (2005).

28 Kuscu, C. *et al.* CRL4-like Clr4 complex in Schizosaccharomyces pombe depends on an exposed surface of Dos1 for heterochromatin silencing. *Proc Natl Acad Sci U S A* **111**, 1795-1800, doi:10.1073/pnas.1313096111 (2014).
29 Thon, G. *et al.* The Clr7 and Clr8 directionality factors and the Pcu4 cullin mediate heterochromatin formation in the fission yeast Schizosaccharomyces pombe. *Genetics* **171**, 1583-1595, doi:10.1534/genetics.105.048298 (2005).
30 Li, F. *et al.* Two novel proteins, dos1 and dos2, interact with rik1 to regulate heterochromatic RNA interference and histone modification. *Curr Biol* **15**, 1448-1457, doi:10.1016/j.cub.2005.07.021 (2005).
31 Irvine, D. V. *et al.* Mapping epigenetic mutations in fission yeast using whole-genome next-generation sequencing. *Genome Res* **19**, 1077-1083, doi:10.1101/gr.089318.108 (2009).
32 Javerzat, J. P., Cranston, G. & Allshire, R. C. Fission yeast genes which disrupt mitotic chromosome segregation when overexpressed. *Nucleic Acids Res* **24**, 4676-4683, doi:10.1093/nar/24.23.4676 (1996).
33 Schalch, T. *et al.* High-affinity binding of Chp1 chromodomain to K9 methylated histone H3 is required to establish centromeric heterochromatin. *Mol Cell* **34**, 36-46, doi:10.1016/j.molcel.2009.02.024 (2009).
34 Ishimoto, K. *et al.* Ubiquitination of Lysine 867 of the Human SETDB1 Protein Upregulates Its Histone H3 Lysine 9 (H3K9) Methyltransferase Activity. *PLoS One* **11**, e0165766, doi:10.1371/journal.pone.0165766 (2016).
35 Sun, L. & Fang, J. E3-Independent Constitutive Monoubiquitination Complements Histone Methyltransferase Activity of SETDB1. *Mol Cell* **62**, 958-966, doi:10.1016/j.molcel.2016.04.022 (2016).
36 Iglesias, N. *et al.* Native Chromatin Proteomics Reveals a Role for Specific Nucleoporins in Heterochromatin Organization and Maintenance. *Mol Cell* **77**, 51-66.e58, doi:10.1016/j.molcel.2019.10.018 (2020).
37 Hoeller, D. *et al.* E3-independent monoubiquitination of ubiquitin-binding proteins. *Mol Cell* **26**, 891-898, doi:10.1016/j.molcel.2007.05.014 (2007).
38 Akoury, E. *et al.* Disordered region of H3K9 methyltransferase Clr4 binds the nucleosome and contributes to its activity. *Nucleic Acids Res* **47**, 6726-6736, doi:10.1093/nar/gkz480 (2019).
39 Iglesias, N. *et al.* Automethylation-induced conformational switch in Clr4 (Suv39h) maintains epigenetic stability. *Nature* **560**, 504-508, doi:10.1038/s41586-018-0398-2 (2018).
40 Zhang, K., Mosch, K., Fischle, W. & Grewal, S. I. Roles of the Clr4 methyltransferase complex in nucleation, spreading and maintenance of heterochromatin. *Nat Struct Mol Biol* **15**, 381-388, doi:10.1038/nsmb.1406 (2008).
41 Ishida, M. *et al.* Intrinsic nucleic acid-binding activity of Chp1 chromodomain is required for heterochromatic gene silencing. *Mol Cell* **47**, 228-241, doi:10.1016/j.molcel.2012.05.017 (2012).

42 Kagansky, A. *et al.* Synthetic heterochromatin bypasses RNAi and centromeric repeats to establish functional centromeres. *Science* **324**, 1716-1719, doi:10.1126/science.1172026 (2009).
43 Holla, S. *et al.* Positioning Heterochromatin at the Nuclear Periphery Suppresses Histone Turnover to Promote Epigenetic Inheritance. *Cell* **180**, 150-164.e115, doi:10.1016/j.cell.2019.12.004 (2020).
44 Ragunathan, K., Jih, G. & Moazed, D. Epigenetics. Epigenetic inheritance uncoupled from sequence-specific recruitment. *Science* **348**, 1258699, doi:10.1126/science.1258699 (2015).
45 Shan, C. M. *et al.* A histone H3K9M mutation traps histone methyltransferase Clr4 to prevent heterochromatin spreading. *Elife* **5**, doi:10.7554/eLife.17903 (2016).
46 Bayne, E. H. *et al.* Stc1: a critical link between RNAi and chromatin modification required for heterochromatin integrity. *Cell* **140**, 666-677, doi:10.1016/j.cell.2010.01.038 (2010).
47 Ban, H., Sun, W., Chen, Y. H., Chen, Y. & Li, F. Dri1 mediates heterochromatin assembly via RNAi and histone deacetylation. *Genetics* **218**, doi:10.1093/genetics/iyab032 (2021).
48 Banani, S. F., Lee, H. O., Hyman, A. A. & Rosen, M. K. Biomolecular condensates: organizers of cellular biochemistry. *Nat Rev Mol Cell Biol* **18**, 285-298, doi:10.1038/nrm.2017.7 (2017).
49 Brangwynne, C. P. *et al.* Germline P granules are liquid droplets that localize by controlled dissolution/condensation. *Science* **324**, 1729-1732, doi:10.1126/science.1172046 (2009).
50 Kato, M. *et al.* Cell-free formation of RNA granules: low complexity sequence domains form dynamic fibers within hydrogels. *Cell* **149**, 753-767, doi:10.1016/j.cell.2012.04.017 (2012).
51 Rhine, K., Vidaurre, V. & Myong, S. RNA Droplets. *Annu Rev Biophys* **49**, 247-265, doi:10.1146/annurev-biophys-052118-115508 (2020).
52 Rippe, K. Liquid-Liquid Phase Separation in Chromatin. *Cold Spring Harb Perspect Biol* **14**, doi:10.1101/cshperspect.a040683 (2022).
53 Weber, S. C. & Brangwynne, C. P. Getting RNA and protein in phase. *Cell* **149**, 1188-1191, doi:10.1016/j.cell.2012.05.022 (2012).
54 Molliex, A. *et al.* Phase separation by low complexity domains promotes stress granule assembly and drives pathological fibrillization. *Cell* **163**, 123-133, doi:10.1016/j.cell.2015.09.015 (2015).
55 Mittag, T. & Parker, R. Multiple Modes of Protein-Protein Interactions Promote RNP Granule Assembly. *J Mol Biol* **430**, 4636-4649, doi:10.1016/j.jmb.2018.08.005 (2018).
56 Gibson, B. A. *et al.* Organization of Chromatin by Intrinsic and Regulated Phase Separation. *Cell* **179**, 470-484.e421, doi:10.1016/j.cell.2019.08.037 (2019).
57 Larson, A. G. *et al.* Liquid droplet formation by HP1α suggests a role for phase separation in heterochromatin. *Nature* **547**, 236-240, doi:10.1038/nature22822 (2017).

58 Sabari, B. R. *et al.* Coactivator condensation at super-enhancers links phase separation and gene control. *Science* **361**, doi:10.1126/science.aar3958 (2018).
59 Strom, A. R. *et al.* Phase separation drives heterochromatin domain formation. *Nature* **547**, 241-245, doi:10.1038/nature22989 (2017).
60 Wang, L. *et al.* Histone Modifications Regulate Chromatin Compartmentalization by Contributing to a Phase Separation Mechanism. *Mol Cell* **76**, 646-659.e646, doi:10.1016/j.molcel.2019.08.019 (2019).
61 Sanulli, S. *et al.* HP1 reshapes nucleosome core to promote phase separation of heterochromatin. *Nature* **575**, 390-394, doi:10.1038/s41586-019-1669-2 (2019).
62 Shin, Y. & Brangwynne, C. P. Liquid phase condensation in cell physiology and disease. *Science* **357**, doi:10.1126/science.aaf4382 (2017).
63 Alberti, S., Gladfelter, A. & Mittag, T. Considerations and Challenges in Studying Liquid-Liquid Phase Separation and Biomolecular Condensates. *Cell* **176**, 419-434, doi:10.1016/j.cell.2018.12.035 (2019).
64 Kroschwald, S. *et al.* Promiscuous interactions and protein disaggregases determine the material state of stress-inducible RNP granules. *Elife* **4**, e06807, doi:10.7554/eLife.06807 (2015).
65 Canzio, D. *et al.* Chromodomain-mediated oligomerization of HP1 suggests a nucleosome-bridging mechanism for heterochromatin assembly. *Mol Cell* **41**, 67-81, doi:10.1016/j.molcel.2010.12.016 (2011).
66 Hinde, E., Cardarelli, F. & Gratton, E. Spatiotemporal regulation of Heterochromatin Protein 1-alpha oligomerization and dynamics in live cells. *Sci Rep* **5**, 12001, doi:10.1038/srep12001 (2015).
67 Müller-Ott, K. *et al.* Specificity, propagation, and memory of pericentric heterochromatin. *Mol Syst Biol* **10**, 746, doi:10.15252/msb.20145377 (2014).
68 Elbaum-Garfinkle, S. *et al.* The disordered P granule protein LAF-1 drives phase separation into droplets with tunable viscosity and dynamics. *Proc Natl Acad Sci U S A* **112**, 7189-7194, doi:10.1073/pnas.1504822112 (2015).
69 Maharana, S. *et al.* RNA buffers the phase separation behavior of prion-like RNA binding proteins. *Science* **360**, 918-921, doi:10.1126/science.aar7366 (2018).
70 Van Lindt, J. *et al.* F/YGG-motif is an intrinsically disordered nucleic-acid binding motif. *RNA Biol* **19**, 622-635, doi:10.1080/15476286.2022.2066336 (2022).
71 Oya, E. *et al.* H3K14 ubiquitylation promotes H3K9 methylation for heterochromatin assembly. *EMBO Rep* **20**, e48111, doi:10.15252/embr.201948111 (2019).
72 Aagaard, L. *et al.* Functional mammalian homologues of the Drosophila PEV-modifier Su(var)3-9 encode centromere-associated proteins which complex with the heterochromatin component M31. *Embo j* **18**, 1923-1938, doi:10.1093/emboj/18.7.1923 (1999).
73 Yamamoto, K. & Sonoda, M. Self-interaction of heterochromatin protein 1 is required for direct binding to histone methyltransferase, SUV39H1. *Biochem Biophys Res Commun* **301**, 287-292, doi:10.1016/s0006-291x(02)03021-8 (2003).

74 Pidoux, A. L., Uzawa, S., Perry, P. E., Cande, W. Z. & Allshire, R. C. Live analysis of lagging chromosomes during anaphase and their effect on spindle elongation rate in fission yeast. *J Cell Sci* **113 Pt 23**, 4177-4191, doi:10.1242/jcs.113.23.4177 (2000).
75 Braun, S. *et al.* The Cul4-Ddb1(Cdt)² ubiquitin ligase inhibits invasion of a boundary-associated antisilencing factor into heterochromatin. *Cell* **144**, 41-54, doi:10.1016/j.cell.2010.11.051 (2011).
76 Trewick, S. C., Minc, E., Antonelli, R., Urano, T. & Allshire, R. C. The JmjC domain protein Epe1 prevents unregulated assembly and disassembly of heterochromatin. *Embo j* **26**, 4670-4682, doi:10.1038/sj.emboj.7601892 (2007).
77 Zofall, M. & Grewal, S. I. Swi6/HP1 recruits a JmjC domain protein to facilitate transcription of heterochromatic repeats. *Mol Cell* **22**, 681-692, doi:10.1016/j.molcel.2006.05.010 (2006).
78 Keller, C., Kulasegaran-Shylini, R., Shimada, Y., Hotz, H. R. & Bühler, M. Noncoding RNAs prevent spreading of a repressive histone mark. *Nat Struct Mol Biol* **20**, 994-1000, doi:10.1038/nsmb.2619 (2013).
79 Kim, H. S. *et al.* Identification of a BET family bromodomain/casein kinase II/TAF-containing complex as a regulator of mitotic condensin function. *Cell Rep* **6**, 892-905, doi:10.1016/j.celrep.2014.01.029 (2014).
80 Wang, J. *et al.* Epe1 recruits BET family bromodomain protein Bdf2 to establish heterochromatin boundaries. *Genes Dev* **27**, 1886-1902, doi:10.1101/gad.221010.113 (2013).
81 Komander, D., Clague, M. J. & Urbé, S. Breaking the chains: structure and function of the deubiquitinases. *Nat Rev Mol Cell Biol* **10**, 550-563, doi:10.1038/nrm2731 (2009).
82 Leznicki, P. & Kulathu, Y. Mechanisms of regulation and diversification of deubiquitylating enzyme function. *J Cell Sci* **130**, 1997-2006, doi:10.1242/jcs.201855 (2017).
83 Reyes-Turcu, F. E., Zhang, K., Zofall, M., Chen, E. & Grewal, S. I. Defects in RNA quality control factors reveal RNAi-independent nucleation of heterochromatin. *Nat Struct Mol Biol* **18**, 1132-1138, doi:10.1038/nsmb.2122 (2011).
84 Ryan, C. J. *et al.* Hierarchical modularity and the evolution of genetic interactomes across species. *Mol Cell* **46**, 691-704, doi:10.1016/j.molcel.2012.05.028 (2012).
85 Liu, Y. *et al.* Functional characterization of the Arabidopsis ubiquitin-specific protease gene family reveals specific role and redundancy of individual members in development. *Plant J* **55**, 844-856, doi:10.1111/j.1365-313X.2008.03557.x (2008).
86 Bühler, M., Spies, N., Bartel, D. P. & Moazed, D. TRAMP-mediated RNA surveillance prevents spurious entry of RNAs into the Schizosaccharomyces pombe siRNA pathway. *Nat Struct Mol Biol* **15**, 1015-1023, doi:10.1038/nsmb.1481 (2008).

87 Kuzdere, T. *et al.* Differential phosphorylation of Clr4(SUV39H) by Cdk1 accompanies a histone H3 methylation switch that is essential for gametogenesis. *EMBO Rep*, e55928, doi:10.15252/embr.202255928 (2022).
88 Babu, M. M. The contribution of intrinsically disordered regions to protein function, cellular complexity, and human disease. *Biochem Soc Trans* **44**, 1185-1200, doi:10.1042/bst20160172 (2016).
89 Bah, A. & Forman-Kay, J. D. Modulation of Intrinsically Disordered Protein Function by Post-translational Modifications. *J Biol Chem* **291**, 6696-6705, doi:10.1074/jbc.R115.695056 (2016).
90 Bah, A. *et al.* Folding of an intrinsically disordered protein by phosphorylation as a regulatory switch. *Nature* **519**, 106-109, doi:10.1038/nature13999 (2015).
91 Oldfield, C. J. & Dunker, A. K. Intrinsically disordered proteins and intrinsically disordered protein regions. *Annu Rev Biochem* **83**, 553-584, doi:10.1146/annurev-biochem-072711-164947 (2014).
92 Qamar, S. *et al.* FUS Phase Separation Is Modulated by a Molecular Chaperone and Methylation of Arginine Cation-π Interactions. *Cell* **173**, 720-734.e715, doi:10.1016/j.cell.2018.03.056 (2018).
93 Stowell, J. A. W. *et al.* A low-complexity region in the YTH domain protein Mmi1 enhances RNA binding. *J Biol Chem* **293**, 9210-9222, doi:10.1074/jbc.RA118.002291 (2018).
94 Yang, P. *et al.* G3BP1 Is a Tunable Switch that Triggers Phase Separation to Assemble Stress Granules. *Cell* **181**, 325-345.e328, doi:10.1016/j.cell.2020.03.046 (2020).
95 Keller, C. *et al.* HP1(Swi6) mediates the recognition and destruction of heterochromatic RNA transcripts. *Mol Cell* **47**, 215-227, doi:10.1016/j.molcel.2012.05.009 (2012).
96 Johnson, W. L. *et al.* RNA-dependent stabilization of SUV39H1 at constitutive heterochromatin. *Elife* **6**, doi:10.7554/eLife.25299 (2017).
97 Shirai, A. *et al.* Impact of nucleic acid and methylated H3K9 binding activities of Suv39h1 on its heterochromatin assembly. *Elife* **6**, doi:10.7554/eLife.25317 (2017).
98 Velazquez Camacho, O. *et al.* Major satellite repeat RNA stabilize heterochromatin retention of Suv39h enzymes by RNA-nucleosome association and RNA:DNA hybrid formation. *Elife* **6**, doi:10.7554/eLife.25293 (2017).
99 Gerace, E. L., Halic, M. & Moazed, D. The methyltransferase activity of Clr4Suv39h triggers RNAi independently of histone H3K9 methylation. *Mol Cell* **39**, 360-372, doi:10.1016/j.molcel.2010.07.017 (2010).
100 Bühler, M., Verdel, A. & Moazed, D. Tethering RITS to a nascent transcript initiates RNAi- and heterochromatin-dependent gene silencing. *Cell* **125**, 873-886, doi:10.1016/j.cell.2006.04.025 (2006).
101 Al-Sady, B., Madhani, H. D. & Narlikar, G. J. Division of labor between the chromodomains of HP1 and Suv39 methylase enables coordination of heterochromatin spread. *Mol Cell* **51**, 80-91, doi:10.1016/j.molcel.2013.06.013 (2013).

102 Chang, A. Y., Castel, S. E., Ernst, E., Kim, H. S. & Martienssen, R. A. The Conserved RNA Binding Cyclophilin, Rct1, Regulates Small RNA Biogenesis and Splicing Independent of Heterochromatin Assembly. *Cell Rep* **19**, 2477-2489, doi:10.1016/j.celrep.2017.05.086 (2017).

103 Bähler, J. *et al.* Heterologous modules for efficient and versatile PCR-based gene targeting in Schizosaccharomyces pombe. *Yeast* **14**, 943-951, doi:10.1002/(sici)1097-0061(199807)14:10<943::Aid-yea292>3.0.Co;2-y (1998).

104 Murray, J. M., Watson, A. T. & Carr, A. M. Transformation of Schizosaccharomyces pombe: Lithium Acetate/ Dimethyl Sulfoxide Procedure. *Cold Spring Harb Protoc* **2016**, pdb.prot090969, doi:10.1101/pdb.prot090969 (2016).

105 Winston, F. EMS and UV mutagenesis in yeast. *Curr Protoc Mol Biol* **Chapter 13**, Unit 13.13B, doi:10.1002/0471142727.mb1303bs82 (2008).

106 Roche, B., Arcangioli, B. & Martienssen, R. A. RNA interference is essential for cellular quiescence. *Science* **354**, doi:10.1126/science.aah5651 (2016).

107 Langmead, B. & Salzberg, S. L. Fast gapped-read alignment with Bowtie 2. *Nat Methods* **9**, 357-359, doi:10.1038/nmeth.1923 (2012).

108 Garrison, E. & Marth, G. Haplotype-based variant detection from short-read sequencing. *arXiv e-prints*, arXiv:1207.3907 (2012). <https://ui.adsabs.harvard.edu/abs/2012arXiv1207.3907G>.

109 Langmead, B., Trapnell, C., Pop, M. & Salzberg, S. L. Ultrafast and memory-efficient alignment of short DNA sequences to the human genome. *Genome Biol* **10**, R25, doi:10.1186/gb-2009-10-3-r25 (2009).

110 Quinlan, A. R. & Hall, I. M. BEDTools: a flexible suite of utilities for comparing genomic features. *Bioinformatics* **26**, 841-842, doi:10.1093/bioinformatics/btq033 (2010).

111 Keller, A., Nesvizhskii, A. I., Kolker, E. & Aebersold, R. Empirical statistical model to estimate the accuracy of peptide identifications made by MS/MS and database search. *Anal Chem* **74**, 5383-5392, doi:10.1021/ac025747h (2002).

112 Nesvizhskii, A. I., Keller, A., Kolker, E. & Aebersold, R. A statistical model for identifying proteins by tandem mass spectrometry. *Anal Chem* **75**, 4646-4658, doi:10.1021/ac0341261 (2003).

113 Wang, H. *et al.* Rubisco condensate formation by CcmM in β-carboxysome biogenesis. *Nature* **566**, 131-135, doi:10.1038/s41586-019-0880-5 (2019).

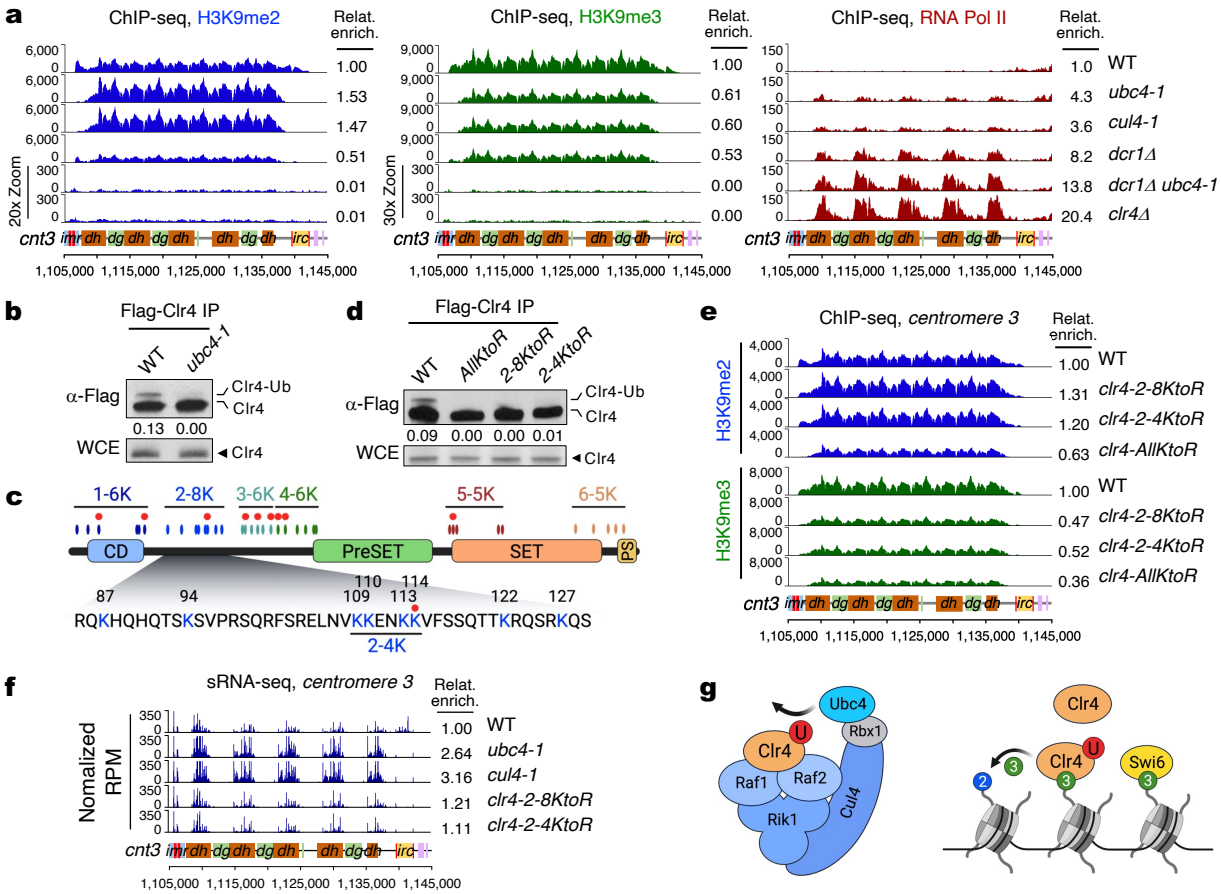

Fig. 1. Mono-ubiquitination of Clr4 by Ubc4-CLRC is required for H3K9me2 to H3K9me3 transition.
a, Chromatin immunoprecipitation and sequencing (ChIP-seq) reads for H3K9me2 (blue), H3K9me3 (green) and RNA Pol II (Rpb1, red) were mapped to centromere 3 (*cnt3*) right arm in the indicated strains. Relative enrichments of ChIP-seq reads from each strain were divided by the total count of WT. Scales for *dcr1Δ ubc4-1* and *clr4Δ* H3K9me2 and 3 were expanded to visualize low reads. A schematic diagram of chromosome *centromere 3* right arm showing innermost repeat (*imr*), outermost repeats (*dg*, *dh*) and boundary region (*irc*) is shown. Vertical red lines and pink boxes represent tRNA and euchromatic genes respectively.
b and **d**, Western blot (WB) analyses of immunoprecipitated Flag-Clr4 (Flag-Clr4 IP) in the indicated strains. The ratio of ubiquitinated Clr4 (Clr4-Ub) compared to unmodified Clr4 is indicated below each lane. Bottom, WB analysis of Flag-Clr4 from whole cell extract (WCE).
c, Schematic diagram of domain structure of Clr4 protein and the position of lysine residues. Ovals show the position of all 36 lysines of Clr4, which are arranged in 6 sub-groups. The second sub-group (2-8K) is highlighted and amino acid sequences are shown. 2-4K sub-group includes K109-K114. Red dots represent putative mono-ubiquitination sites identified by *in vitro* ubiquitination and Mass Spec analyses. CD: chromodomain, PS: PostSET.
e, ChIP-seq reads of H3K9me2 (blue) and H3K9me3 (green) mapped to chromosome 3 centromere right arm in the indicated strains.
f, sRNA-seq reads mapped to centromere 3 right arm in indicated strains.
g, Left, schematic diagram showing the presumptive subunit arrangement in the complex of Ubc4-CLRC and its substrate Clr4 for mono-ubiquitination. Red circle (U), ubiquitin. Right, model for the binding of Clr4 and Swi6 to existing H3K9me3 and the activity of Clr4 for converting H3K9me2 to H3K9me3. Blue circle, H3K9me2 and green circle, H3K9me3.

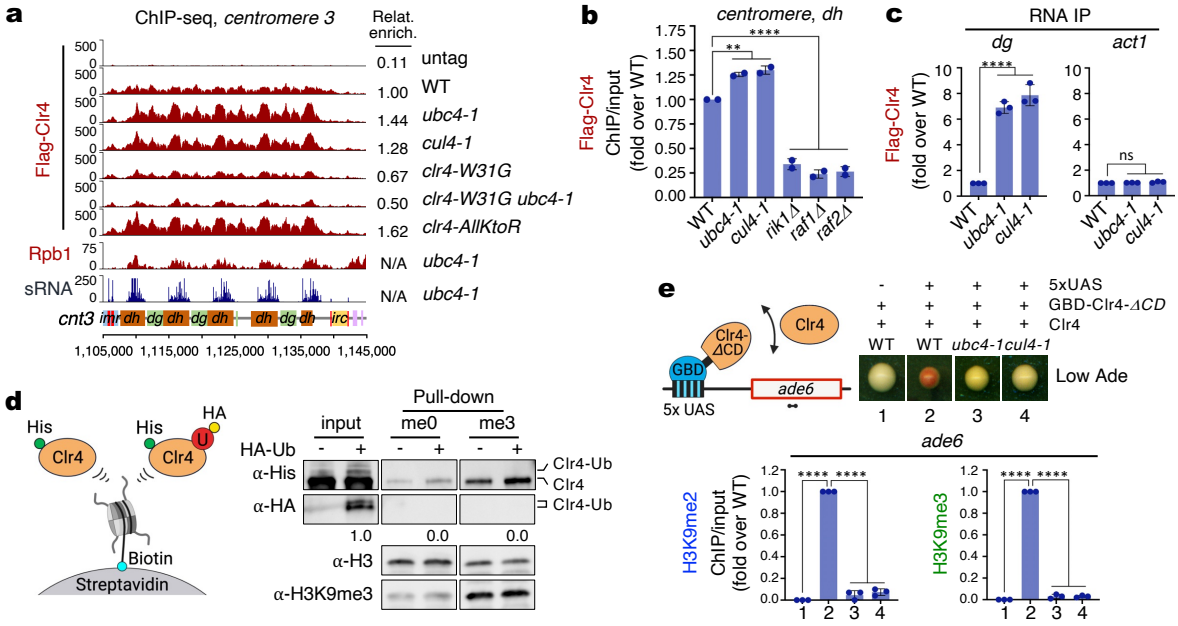

Fig. 2. Clr4 mono-ubiquitination induces its dissociation from chromatin and from centromeric ncRNA.
a, ChIP-seq reads of Flag-Clr4 and RNA Pol II (Rpb1) and sRNA-seq reads mapped to chromosome 3 centromere (*cnt3*) right arm in indicated strains. N/A, not available.
b, ChIP-qPCR assay showing enrichment of Flag-Clr4 at centromeric *dh* repeat in the indicated strains. Error bars, S.D. (n = 2). *P* values are from Dunnett's multiple comparisons tests. $P = 0.0026$ for *ubc4-1*, $P = 0.0011$ for *cul4-1* and $P < 0.0001$ for *rik1Δ, raf1Δ* and *raf2Δ*.
c, RNA immunoprecipitation (RNA IP) and qPCR of Flag-Clr4 to centromeric *dg* and *act1* transcript in the indicated strains. Error bars, S.D. (n = 3). *P* values are from Dunnett's multiple comparisons tests. $P < 0.0001$ for *ubc4-1* and *cul4-1* (*dg,* left). ns, not significant (*act1*, right).
d, Binding assay of *in vitro* ubiquitinated His-Clr4 protein with nucleosomes with unmodified histone H3 (me0) or H3K9me3 histone (me3) anchored to streptavidin beads. Input and His-Clr4 proteins from pull-down were analyzed by WB analyses using antibodies as shown. U, ubiquitin. HA-Ub, HA-ubiquitin. Schematic diagram (left).
e, Schematic diagram for tethering of GBD-Clr4-*ΔCD* to 5xUAS-ade6 locus with free Clr4 protein. Primers for ChIP-qPCR are indicated (left). Right, assay for silencing of *ade6* on Low Ade medium in the indicated strains. Silencing (red color) depends on Ubc4 and Cul4. Bottom, ChIP-qPCR assays showing enrichment of H3K9me2 and H3K9me3 at *ade6* in the indicated strains. Error bars, S.D. (n = 3). *P* values are from Dunnett's multiple comparisons tests. $P < 0.0001$ for 2, 3 and 4 (H3K9me2, Left). $P < 0.0001$ for 2, 3 and 4 (H3K9me3, Right).

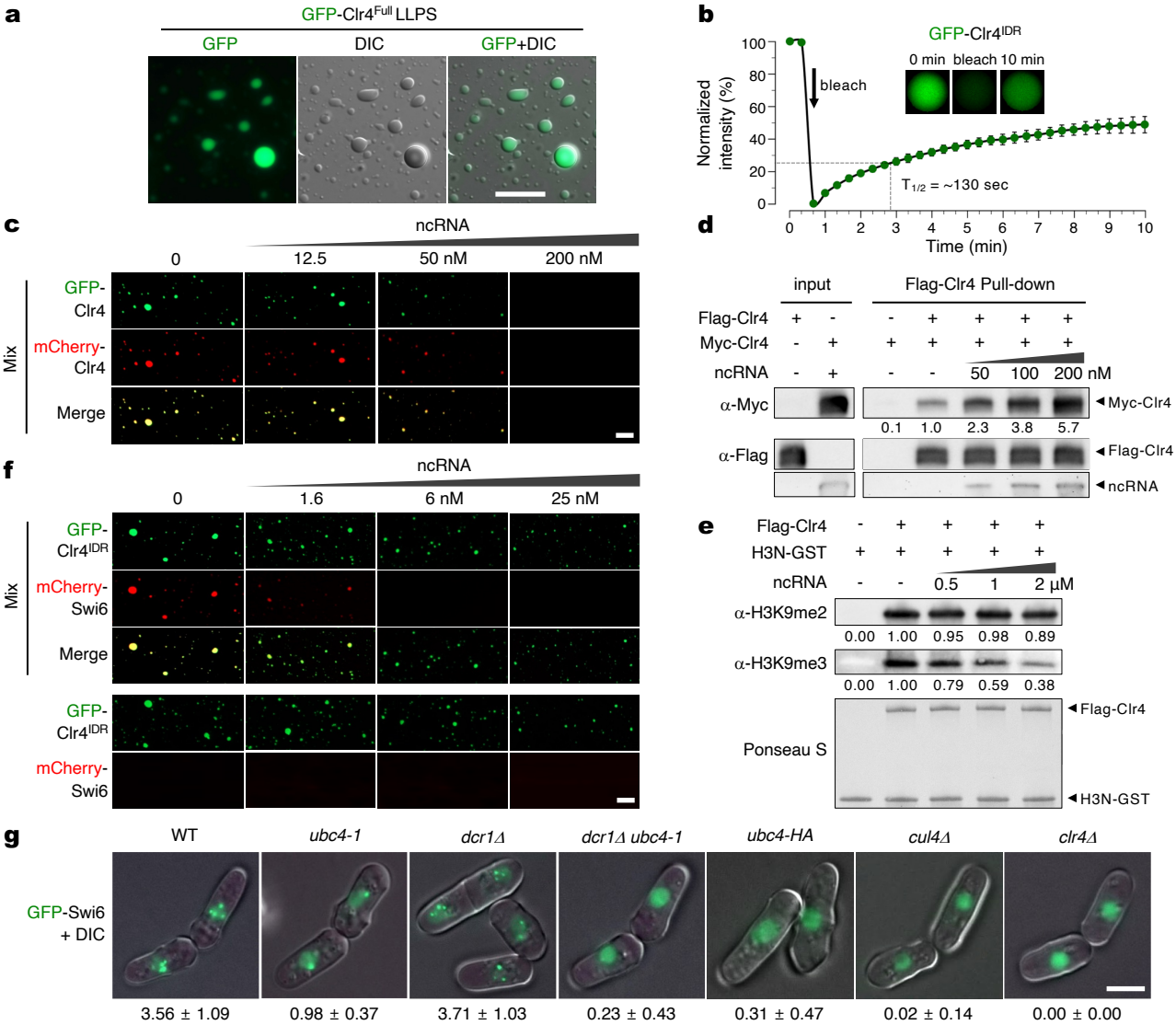

Fig. 3. Phase separation of Clr4 is inhibited by non-coding RNA.

a, Representative images of phase-separated liquid droplets of GFP-Clr4^{Full} protein. DIC; Differential interference contrast. Scale bar, 5 μm.

b, FRAP (Fluorescence Recovery After Photobleaching) of GFP-Clr4^{IDR} before and after bleaching. The change of fluorescence was analyzed in mean and S.D. (n = 5). Arrow shows the time of bleaching (~40 s) and halftime of recovery ($T_{1/2}$) is shown. Representative images at times of 0 min, bleaching (~40 s) and 10 min are shown.

c, Representative images of phase-separated liquid droplets of mixed GFP-Clr4 and mCherry-Clr4 (500 nM of each), in the presence of different amount of centromeric ncRNA. Scale bar, 5 μm.

d, *In vitro* pull down assay for Flag-Clr4 with Myc-Clr4 (500 nM of each) in the presence of increasing amounts of centromeric ncRNA. WB analyses of input and precipitated proteins are shown. The ratio of Myc-Clr4 precipitated by Flag-Clr4 in the absence of ncRNA was set to 1. ncRNA was stained with SYBR Gold.

e, *In vitro* histone methylation (HMT) assay. Recombinant H3N-GST (10 μM) was used in HMT assay with Flag-Clr4 (5 μM) in the absence and presence of ncRNA. WB analyses were carried out using H3K9me2 and H3K9me3 antibodies. Ponceau S staining of the blot is shown in the bottom.

f, Representative images of phase-separated liquid droplets of GFP-Clr4^{IDR} mixed with mCherry-Swi6 and unmixed GFP-Clr4^{IDR} and mCherry-Swi6 (bottom, 500 nM of each), in the presence of different amount of centromeric ncRNA. Scale bar, 5 μm.

g, Live cell imaging showing condensed GFP-Swi6 heterochromatic foci in indicated strains. Condensates are lost in strong alleles of *dcr1Δ ubc4-1, ubc4-HA*, *cul4Δ* as well as *clr4Δ* mutants. Scale bar, 2.5 μm. The average number of GFP-Swi6 condensates are indicated below each panel. S.D. (n > 50).

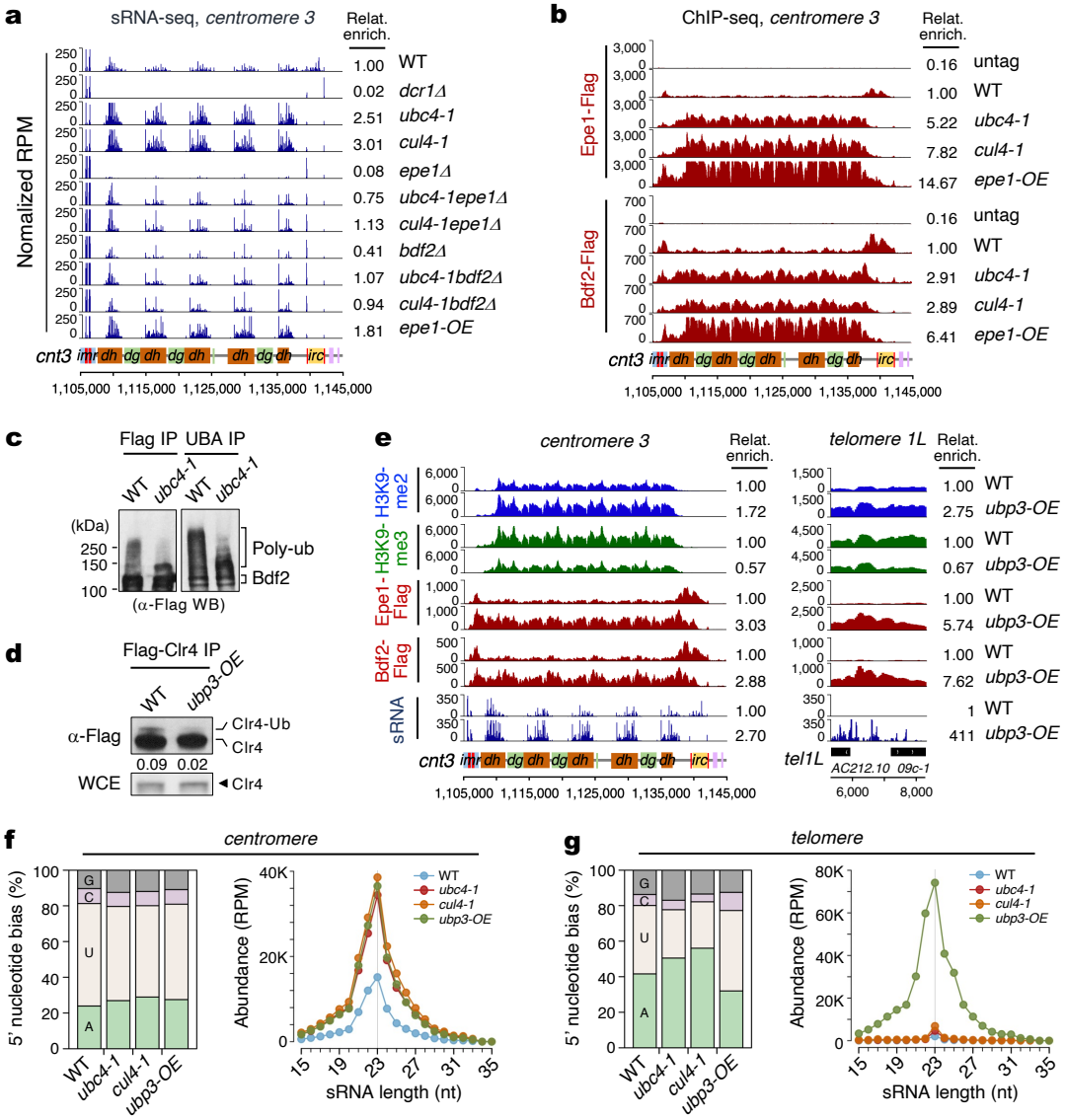

Fig. 4. Ubiquitination and de-ubiquitination of Epe1 and Bdf2^{BRD4} regulates centromeric sRNA and Clr4 for heterochromatin silencing.

a, sRNA-seq reads were mapped to centromere 3 right arm. Remaining sRNA peaks in *dcr1Δ* are tRNA-related products. Total counts of sRNA reads without tRNA from different strains were divided by total count of WT. *epe1-OE*, *epe1* overexpression strain. Epe1 is a putative H3K9me3 demethylase.

b, ChIP-seq reads of Epe1-Flag and Bdf2-Flag mapped to chromosome 3 centromere (*cnt3*) right arm in the indicated strains. Bdf2 is the homolog of the human co-transcriptional activator BRD4.

c, WB analyses of immunoprecipitated Bdf2-3xFlag (Flag IP) from WT and *ubc4-1* mutant cells treated with proteasome inhibitor MG-132 (100 μM) for 4 h before harvest (left). Bdf2-3xFlag enrichment by ubiquitination affinity beads (UBA IP) are shown on right.

d, WB analyses of immunoprecipitated Flag-Clr4 (Flag-Clr4 IP) in the indicated strains. *Ubp3-OE*, de-ubiquitinase *ubp3* overexpression strain.

e, ChIP-seq of H3K9me2, H3K9me3, Epe1-Flag and Bdf2-flag and sRNA-seq reads at centromere (left) and telomere (right) in the indicated strains.

f and **g**, 5'-nucleotide composition (left) and size distribution (right) of centromeric sRNAs (**f**) and telomeric sRNAs (**g**) in the indicated strains.